ADVANCED FUNCTIONAL MATERIALS
www.afm-journal.de

Surface Rutilization of Anatase TiO_2 Nanorods for Creation of Synergistically Bridging and Fencing Electron Highways

Jiazang Chen, Hong Bin Yang, Hua Bing Tao, Liping Zhang, Jianwei Miao, Hsin-Yi Wang, Junze Chen, Hua Zhang, and Bin Liu**

In a photoelectrochemical cell, the most concerned issue in the nanostructured TiO_2 electrode is the charge transport, which consists of the internal movement of electrons in TiO_2 nanostructures and the intergrain charge transfer. Here, inspired by electrochemical studies on different polymorphs of TiO_2, it is proposed to bridge the adjacent building blocks and fence the electron transport highways in TiO_2 electrodes by surface rutilization of anatase nanorods. The ultrathin rutilized layer completely coated on the anatase surface has a slightly higher conduction band edge than that of anatase. The obtained surface rutilized anatase nanorods can not only improve the intergrain charge transfer while maintaining fast electron transport within anatase but also minimize the internal energy consumption and protect the electrons in TiO_2 electrodes from recombination, which are beneficial to the charge collection and can significantly improve the photovoltaic performance of photoelectrochemical cells.

1. Introduction

As known, TiO_2 is the most widely used semiconductor material in photoelectrochemical (PEC) applications owing to its unique electrical and optical characteristics which could offer superior performances in photovoltaic devices, water splitting cells, and so on.[1] Rutile and anatase are the most common phases of TiO_2. Although the anatase TiO_2-based PEC systems usually exhibit better performance compared to the rutile TiO_2, the emerging of the synergistic effect between these two polymorphs becomes a promising pathway to design more efficient electrodes/catalysts.[2]

Despite the intensive studies, there is no generally accepted experimental evidence to clarify the intrinsic difference related to PEC behaviors between these two polymorphs.[3] Explanations for the observation that anatase is superior to rutile in PEC cells are mainly based on the theoretically higher charge mobility and longer excited-state lifetime of anatase.[4] Moreover, the band alignment between anatase and rutile used to explain their synergistic effect is also under controversy.[5] The lack of credible proof to discriminate the intrinsic differences between these two polymorphs becomes a bottleneck to design efficient TiO_2 electrodes/catalysts to take good use of the synergistic effect.

In the PEC application, TiO_2 electrodes are usually made of nanostructures.[1a,6] In this situation, it is not rational to apply the physical parameters obtained from the bulk crystalline materials to explain the phenomena in PEC systems, in which the electronic processes and band structures of the semiconductors are sensitively affected by certain factors, such as the ingredient of electrolyte, the density of (photo)-electrochemically doped electrons, and in particular the construction of electrodes.[6,7] For example, due to grain boundary scattering, the charge mobility in field-free electrodes is usually three orders of magnitude smaller than that in bulk crystals.[8] In this case, the boundary scattering plays a crucial role in charge mobility.[8d,8e] Therefore, the transport of charges in mesoporous electrodes will be no longer solely predominated by the "internal charge movement," since the "intergrain charge transfer" also plays a profound role in the charge diffusion. Furthermore, the electronic processes occurred in PEC cells are rather environment dependent. Since the physical methods like X-ray photoemission and Hall Effect techniques for the TiO_2 test are carried out under "dry ambient conditions," certain factors like band edge movement and charge depletion are ignored. In addition, in certain electrochemical and/or PEC systems like photovoltaic devices, the charge recombination usually reflects the transfer of extrinsically given electrons from the semiconductor to the electron acceptors (oxidized species) in the electrolyte, rather than the annihilation of the pairs of intrinsic positive and negative charges in the excited states.[9] Therefore, the application of parameters obtained from boundary-less bulk crystals using "dry physical methods" to explain the better performance of anatase TiO_2-based PEC cells is somehow intuitive and result-oriented, which cannot give us satisfied elucidation, nor provide valuable information to consciously utilize the synergistic effect.

Dr. J. Chen, Dr. H. B. Yang, H. B. Tao, Dr. J. Miao, H.-Y. Wang, Prof. B. Liu
School of Chemical and Biomedical Engineering
Nanyang Technological University
62 Nanyang Drive, Singapore 637459, Singapore
E-mail: liubin@ntu.edu.sg
L. Zhang, J. Chen, Prof. H. Zhang
Center for Programmable Materials
School of Materials Sciences and Engineering
Nanyang Technological University
50 Nanyang Avenue, Singapore 639798, Singapore
E-mail: hzhang@ntu.edu.sg

DOI: 10.1002/adfm.201504105

Here, based on the electrochemical study on the difference between rutile and anatase TiO_2 in PEC systems, we propose to rutilize the surface of anatase TiO_2 nanostructures to reduce the energy consumption during the electronic processes and save the charge from recombination. We first investigate the polymorph differences by comparing the parameters of electronic processes occurred in porous TiO_2 electrodes made of these two polymorphs. To eliminate the interference of architectural effect and obtain reliable parameters, we manage to make the shape and size of the nanostructures, as well as the construction of TiO_2 electrodes made of different polymorphs, the same. The promising band alignment between these two polymorphs and the efficient intergrain charge transfer offered by the participation of rutile phase maps the synergistic effect occurred in the electrodes made of surface rutilized anatase TiO_2. The ultrathin rutile layer, which is in situ transformed from the anatase phase and completely covers the surface of anatase nanostructures, can efficiently improve the intergrain electronic connectivity by bridging the adjacent building blocks and protect the charge in the semiconductor from recombination on semiconductor–electrolyte interface (SEI) by fencing the electron transport highways in TiO_2 electrodes.

2. Results and Discussion

2.1. Preparation of Anatase and Rutile TiO_2 Nanorods with Similar Size and Morphology

For nanostructured semiconductor electrodes, the electronic processes, especially the transport of charge, are strongly architecture dependent. Some of their features, including porosity of semiconductor films, morphology of building blocks, and coordination number and necking area between grains in the semiconductor electrodes, can profoundly influence their electronic processes.[8d,8f,10] Among these features, the shape and size of the building blocks are intrinsic. Therefore, in order to obtain reliable parameters for further comparing the difference in the electronic processes occurred in semiconductor electrodes, the preparation of TiO_2 nanostructures of different polymorphs with similar shape and size becomes the prerequisite. Generally, rutile tends to grow into 1D rod-like nanostructures while the preferred shape for anatase is particulate in hydrothermal systems. Recently, the development of thermodynamically driven 1D evolution of anatase inspires us to further explore the synthetic strategy to grow anatase TiO_2 nanostructures with similar shape and size to the rutile counterparts.[10b]

During the hydrothermal growth of anatase TiO_2 nanorods, morphological features including length, diameter, and aspect ratio increase with the ammonia concentration (Figure S1, Supporting Information).[10b] For the rutile counterparts, the features including the aspect ratio are mainly controlled by the kinetics of the linear assembly of sixfold coordinated hydrolyzed monomers by sharing opposite edges in the equatorial of octahedrons.[11] The morphologies of the rutile nanostructures can be tuned by modifying the acidity in reaction and changing the titanium precursors (Figure S2, Supporting Information). Therefore, TiO_2 nanostructures with similar shape and size for these two polymorphs can be obtained by co-adjusting the experimental parameters (see the Experimental Section for details) (**Figure 1** and Figures S3 and S4, Supporting Information).

The anatase and rutile TiO_2 nanostructures used for the investigation of their electrochemical behaviors were characterized by field emission scanning electron microscopy (FESEM) and transmission electron microscopy (TEM). The anatase and rutile TiO_2 nanostructures synthesized by hydrothermal treatment of titanium precursors in alkaline and acidic solutions have very similar shape and size. The FESEM images (Figure 1a) and X-ray diffraction (XRD) patterns (Figure S3, Supporting Information) show that the TiO_2 nanostructures synthesized by hydrothermal treatment of titanium isopropoxide in alcoholic ammonia water system are of rod-like shape and phase-pure anatase with an average diameter of ≈40 nm and length of ≈120 nm. TEM image (Figure 1b) and selected area electron

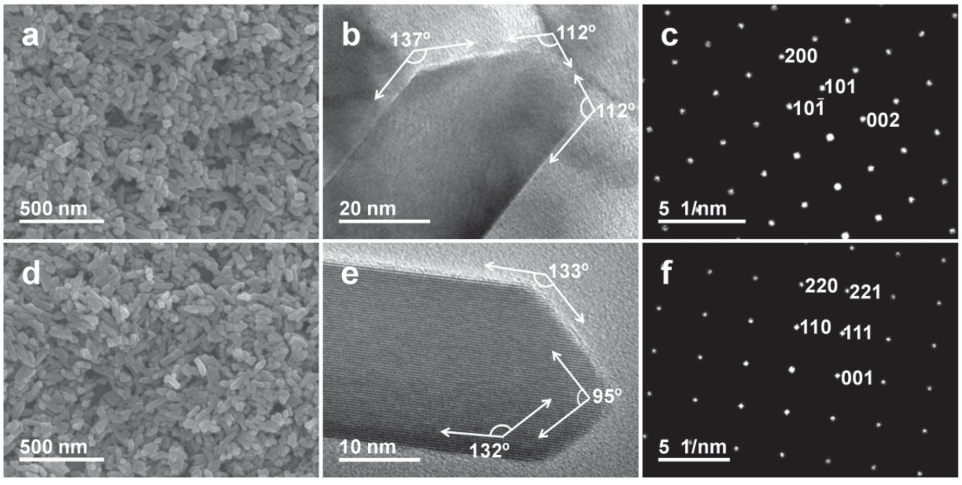

Figure 1. Characteristics of the TiO_2 nanostructures. a) FESEM image, b) TEM image, and c) SAED pattern of the anatase TiO_2 nanorods synthesized by hydrothermal treatment of titanium isopropoxide in an alcoholic ammonia–water system. d) FESEM image, e) TEM image, and f) SAED pattern for the rutile TiO_2 nanorods obtained by hydrothermal treatment of $TiCl_4$ (final concentration of 0.5 M in the reaction autoclave). It can be seen that a,d) the size and b,e) the shape of these two polymorphs of TiO_2 are very similar.

diffraction (SAED) patterns (Figure 1c) further confirmed that the nanorods are single-crystalline anatase and have a distorted quadrilateral shape in the tip. The angles in the tip are 137° and 112°, which can be attributed to the angles between (101) and (–101) planes, and between (101)/(–101) and (002) planes of anatase crystals, respectively (Figure 1b,c). The rutile TiO_2 nanostructures (Figure 1d,e) prepared by hydrothermal treatment of $TiCl_4$ solution have very similar morphology to that of anatase counterparts (Figure 1a,b). Moreover, the SAED (Figure 1f) and XRD patterns (Figure S3, Supporting Information) prove that the rutile TiO_2 nanostructures are phase-pure single-crystalline.

2.2. Electrochemical Investigation of Intrinsic Polymorph Differences

2.2.1. Determination of Trap-Free Diffusion Coefficients

To illustrate the intrinsic difference between the anatase and rutile TiO_2 nanostructure, the electronic processes occurred in the electrodes made of them were investigated by electrochemical impedance spectroscopy. For cells with good carrier collection efficiency, the electron transport in TiO_2 films appears as the Warburg-like diffusion behavior in the high-frequency range and the interfacial charge recombination process grows into a large semicircle in the low-frequency region (Figure S5, Supporting Information).[12] The electronic processes in PEC cells are well described by the transmission line model (Figure S6, Supporting Information).[12,13] By fitting the obtained impedance spectra with the transmission line model,[12,13] we obtained the parameters including electron transport resistance (R_t), interfacial charge recombination resistance (R_{ct}), and chemical capacitance (C_μ) that describe the electronic processes in the semiconductor electrodes.

The propagation of electrons in nanostructured semiconductor electrodes is mainly driven by diffusion, because of the effective electrolyte shielding of space charge.[14] The diffusion coefficient of the electrons within the mesoporous semiconductor electrodes strongly depends on the structural architectures and the density and distribution of the trap states located in the band gap

$$D_n = \frac{1}{1+\frac{\partial n_L}{\partial n_C}} D_0 \tag{1a}$$

where n_L is the trapped electron density and n_C is the conduction band electron density. When the electronic Fermi level (E_F) is far away from the conduction band edge (E_{CB}), namely, $E_F < E_{CB} - k_BT$ (here k_B is the Boltzmann constant and T is the temperature), the term $\partial n_C/\partial n_L$ is small, and then Equation (1a) becomes

$$D_n = \left(\frac{\partial n_C}{\partial n_L}\right) D_0 \tag{1b}$$

The prefactor $\partial n_C/\partial n_L$ reflects the delay of the response of chemical diffusion coefficient by the trapping and detrapping processes. It is therefore elicited that the effective electron diffusion coefficient (D_n) is governed by the density of localized states and the depth of the trap sites. Under quasi steady-state condition, the effective diffusion coefficient of electrons in TiO_2 electrode can be obtained by using small perturbation techniques, such as intensity modulated photocurrent spectroscopy and impedance spectroscopy. Here we calculated D_n from the transport resistance (R_t) and chemical capacitance (C_μ) based on $D_n = \left(R_t C_\mu\right)^{-1}$. D_0 is the constant diffusion coefficient of freely mobile electrons (trap-free charge transport) at or above the transport edge of the semiconductor mesoporous electrodes, which is closely related to the structural architectures and intrinsic property of the semiconductor.[8d] Therefore, the value of D_0 would be a characteristic parameter for a given semiconductor electrode, which provides constructional features, including porosity of semiconductor films, morphology of building blocks, and coordination number and necking area between grains.[8d,8f,10] The chemical diffusion coefficient can be obtained from

$$D_n = \frac{N_C T_0}{N_L T} \cdot \exp\left[\left(E_F - E_C\right) \cdot \left(\frac{1}{k_B T} - \frac{1}{k_B T_0}\right)\right] D_0 \tag{1c}$$

where N_C is the effective density of states in the conduction band, N_L is the total density of the localized states, k_B is the Boltzmann constant, and T_0 is the characteristic temperature which determines the depth and distribution of trap sites below the lower edge of the conduction band. When $E_F \approx E_{CB} - k_BT$, the term $\partial n_C/\partial n_L \geq 1$, the chemical diffusion coefficient of charge is equal to the constant diffusion coefficient ($D_n \approx D_0$, according to Equation (1a). Therefore, the constant diffusion coefficient can be estimated by extrapolating the relationship of D_n–E_F obtained at various temperatures.[8d]

Figure 2 shows the exponential variation of D_n values over the electronic Fermi level at various temperatures. As shown by the D_n–E_F relationship, the electrodes made of rutile and anatase TiO_2 nanostructures with similar architectures (Figure 1 and Figure S7, Supporting Information) exhibit very similar values of trap-free diffusion coefficients. The D_0 values for rutile and anatase TiO_2 electrodes are 0.0104 and 0.0147 $cm^2\ s^{-1}$, respectively, corresponding to 0.402 and 0.568 $cm^2\ V^{-1}\ s^{-1}$ for electron mobility at room temperature. Taking account of the size of our TiO_2 nanostructures, these values of trap-free diffusion coefficient and the related mobility are rational as compared with the reported parameters.[8d,10b]

2.2.2. Band Alignment and Electronic Processes

It has been established that the conductivity of electrons in TiO_2 network is exclusively dependent on the number of free electrons in extended states[15]

$$\sigma = q\mu n \tag{2a}$$

where q is the elementary charge, μ is the mobility, and n is the density of free electrons. For diffusion of charged particles like electrons, the mobility equation can be described as

$$\mu = \frac{qD_0}{k_B T} \tag{2b}$$

Although these electrodes are made of different TiO_2 materials, they would have similar values of conductivity if densities

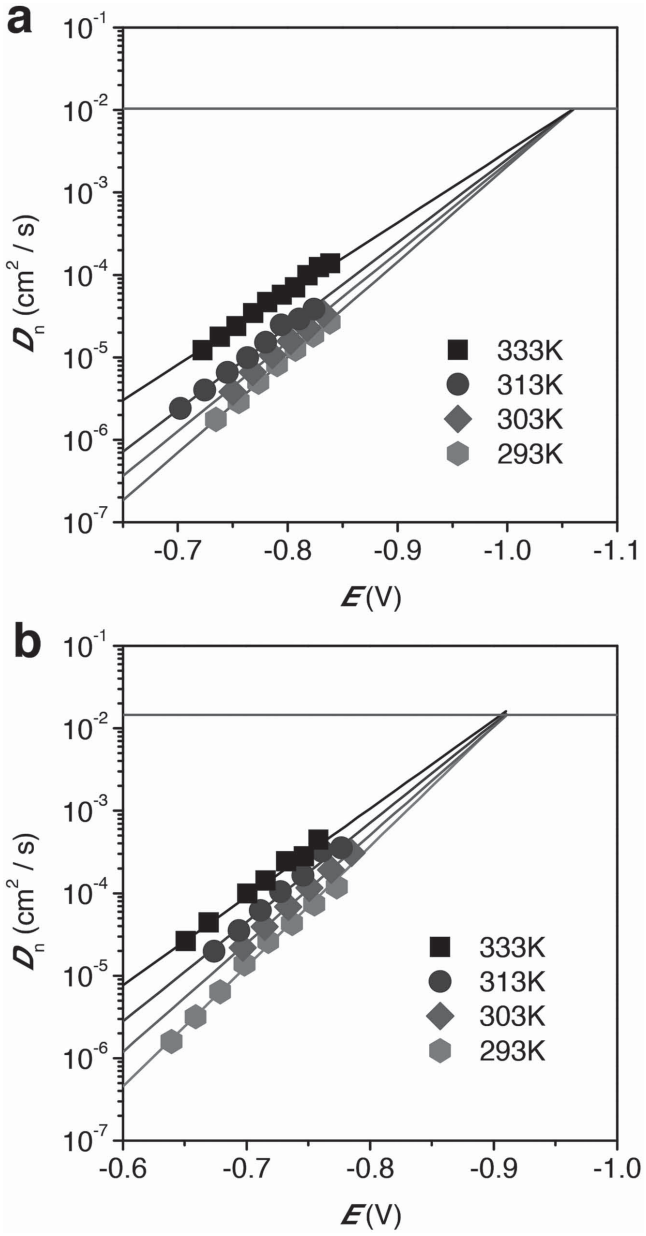

Figure 2. Temperature-dependent diffusion coefficient of electrons in TiO_2 electrodes. Electron diffusion coefficient for a) rutile and b) anatase TiO_2 electrodes over the measured potential range under various temperatures. The trap-free diffusion coefficient (D_0) of electrons in the electrodes can be obtained by extrapolating the D_n plots. The D_0 values for rutile and anatase TiO_2 electrodes are 0.0104 and 0.0147 cm^2 s^{-1}, respectively, corresponding to 0.402 and 0.568 cm^2 V^{-1} s^{-1} for electron mobility. Parameters, such as electronic conductivity, chemical capacitance, and diffusion coefficient D_n in the electrodes, were obtained by fitting and calculating the data from the impedance spectra.

of electrons in the conduction band are kept the same. Therefore, the electronic conductivity can provide a reference for the position of the E_F with respect to the E_{CB}[15,16]

$$\sigma = \sigma_0 \exp\left[-\frac{(E_{CB} - E_F)}{k_B T}\right] \quad (2c)$$

where σ_0 is a constant related to charge mobility. The electronic conductivity is independent of the number of traps, because it is only related to the steady-state transport and reflects the rate of displacement in the transport band.[17] In contrast, the electron diffusion coefficient of semiconductor network is strongly dependent on the occupation of traps.[14] Thus, it is reasonable to take the electron conductivity as a parameter to compare the electrochemical properties of different semiconductor electrodes at the same electron density. The conductivity of TiO_2 network can be calculated from R_t by using the geometrical parameters.

In the redox couple-based PEC and electrochemical cells, e.g., the very exemplificative cells based on I^-/I_3^- couples, the redox potential (E_{redox}) is stationary. The bias potential of the cell is related to the difference between the electronic Fermi level in the TiO_2 and E_{redox}. Therefore, the relationship of potential–conductivity can provide the difference between the E_{CB} of TiO_2 and E_{redox}

$$\sigma = \sigma_0 \exp\left[\frac{q}{k_B T}\left(V + \frac{(E_{Redox} - E_{CB})}{q}\right)\right] \quad (2d)$$

Figure 3a shows the comparison of potential-dependent conductivity of the cells assembled from anatase and rutile TiO_2. Under a similar biased potential (electronic Fermi level), the conductivity of rutile electrode is much smaller than that of anatase. Since the mobility of charges in the two electrodes is similar, the rather high charge transport resistance suggests that the density of free electrons in the rutile electrode is low, as compared to the anatase electrode. According to Equations (2a)–(2d), the lower density of free electrons suggests that the position of conduction band edge for rutile TiO_2 is higher than that of anatase TiO_2 (Figure 3).

Chemical capacitance is proportional to the density of electronic states in the band gap of semiconductor. Figure 3b shows the relationship between chemical capacitance and electrode potential for both the anatase and rutile TiO_2 electrodes. It can be seen that all data points in both the plots lie in almost the same line and have similar slopes over the measured potential range, indicating that the density and distribution characteristic of band tail states below the electronic Fermi level for the anatase and rutile TiO_2 electrodes are very similar (Figure 3b,c). Despite similar electronic states below the electronic Fermi level, the density of trap sites below the conduction band is higher for the rutile electrode (Figure 3c), as compared to that of the anatase electrode. Therefore, the effect of trapping/detrapping events on the charge transport would be more obvious for the rutile electrode.

Our aforementioned inference is rational. The construction features like the porosity of electrodes and the cells used for studying the electronic structures are similar to the widely applied electrochemical and PEC systems, suggesting that our result is of more extensive universality. Besides, our proposed band alignment is in good agreement with the results obtained by Scanlon et al.[5b] and Klein and co-workers[18] who determined the difference of band position for the two polymorphs of TiO_2 by combination of the material simulation techniques and X-ray photoemission experiments.

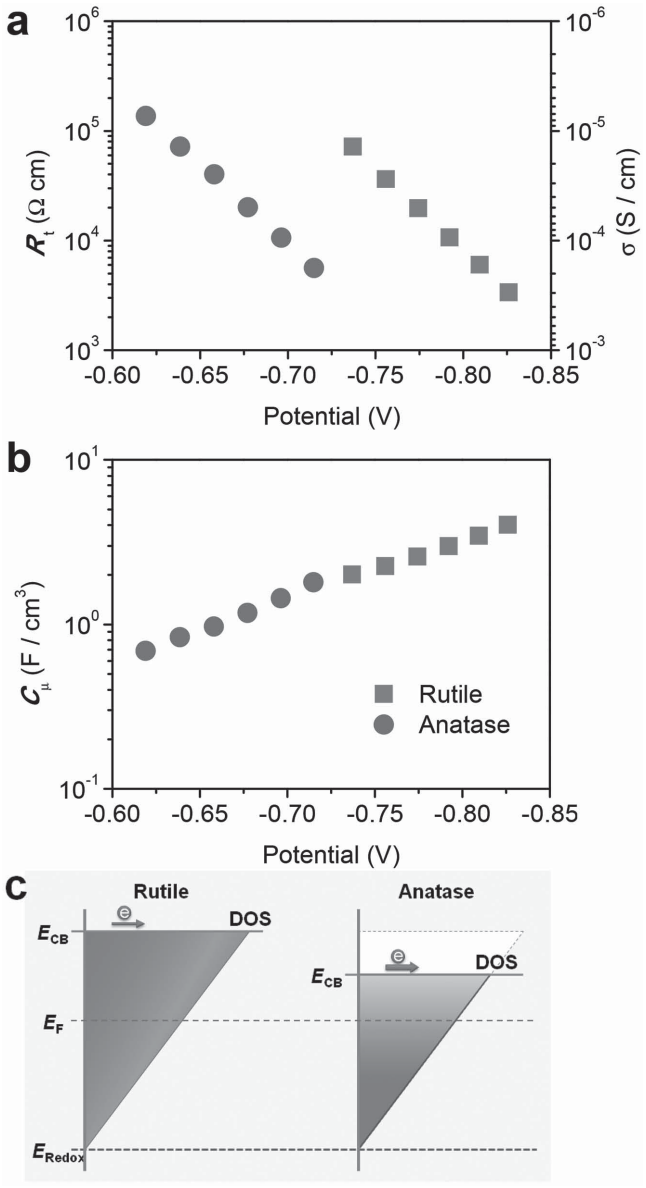

Figure 3. Density and distribution of electronic states in the semiconductor electrodes. a) Charge transport resistance and electronic conductivity and b) chemical capacitance of rutile and anatase TiO_2-based mesoporous electrodes varied along the electrode potentials. c) Schematic illustration for the energetics, and density and distribution of trap states in the TiO_2 electrodes. Although the mobility of electrons in the rutile electrode is slightly lower than that in the anatase one (Figure 2), the difference in their conductivity is more obvious. Therefore, it is safe to conclude that the conduction band edge of rutile is higher than that of anatase (c).

2.2.3. Effect of Trap States on Charge Transport

The distribution of trap states below the conduction band will prolong the charge transport time, according to the multiple trapping (MT) model.[19] In this situation, D_n grows exponentially as E_F shifts toward more negative potential (Figure S8, Supporting Information). For the rutile TiO_2 electrode, the density of trap states below the conduction band is relatively high, as compared to the anatase electrode (Figure 3b,c). Therefore, the rutile electrode shows a smaller electron diffusion coefficient (Figure S8, Supporting Information, and **Figure 4**). Besides, the trap states located at/near the surface of the semiconductor will act as intermediates to trap electrons and increase the probability of charge recombination.[20] The relatively higher density of trap states in the rutile TiO_2 electrode will aggravate the interfacial leakage of charges on the SEI (Figure S9, Supporting Information). By virtue of these benefits like the retarding of interfacial charge recombination for the cells with anatase TiO_2 electrodes, the lifetime (τ_n) and the diffusion length (L_n) of electrons in the semiconductor electrodes can be effectively increased (Figure S10, Supporting Information).

Moreover, due to the larger coefficient for charge diffusion and much longer surviving time for the electrons in the anatase electrodes as well as the ability to travel longer distances (Figures 2 and 4 and Figure S8 and S10, Supporting Information), PEC systems made of anatase electrodes exhibited better charge collection performance. In our photovoltaic devices, i.e., dye-sensitized solar cells (DSSCs), the photocurrent–voltage characteristics (Figure S11, Supporting Information) show that the cell assembled from the rutile TiO_2 electrode gave the short-circuit photocurrent density (J_{SC}) of 10.06 mA cm^{-2}, open-circuit voltage (V_{OC}) of 773 mV, fill factor (FF) of 0.760, and energy conversion efficiency (η) of 5.91%. By replacing the rutile TiO_2 electrode with anatase TiO_2 electrode, the values for J_{SC}, V_{OC}, and FF increase to 14.93 mA cm^{-2}, 783 mV, and 0.763, respectively, with energy conversion efficiency of 8.92%. Although the conduction band edge of anatase TiO_2 is ≈100 mV lower (Figure 3a,c) than that of rutile polymorph, the open-circuit voltages for the two cells (anatase and rutile TiO_2) are similar. Analogous result has also been reported by Frank and co-workers[21] who proposed that the semiconductor electrodes with lower conduction band edge could offer relatively higher voltage by blocking the interfacial charge leakage. Here in our case, the effective suppression of interfacial charge recombination (Figure 4 and Figure S9, Supporting Information) can increase the density of electrons in the anatase TiO_2 electrode and further upshift the electronic Fermi level.

2.3. Bridging and Fencing Electron Highways in Nanostructured Electrodes

2.3.1. Investigation of Intergrain Charge Transfer by Deconvolution of Charge Mobility

It is generally accepted that the charge mobility in crystalline anatase TiO_2 is larger than that in rutile counterpart.[22] For example, the electron mobility in the single-crystalline anatase TiO_2 can reach as high as 10–20 cm^2 V^{-1} s^{-1}, while for the single-crystalline rutile TiO_2, it decreases to 0.1–1 cm^2 V^{-1} s^{-1}. However, the situation is rather different in the porous nanostructured semiconductor electrode. It has been reported that the value of D_0 in nanostructured anatase TiO_2 films is only in the range of 10^{-3}–10^{-2} cm^2 s^{-1}, corresponding to a charge mobility of ≈0.003–0.03 cm^2 V^{-1} s^{-1}, which is approximately three orders of magnitudes less than that in the single-crystalline materials, most likely arising from the "intergrain scattering."[8] Since the charge transport takes place in both the

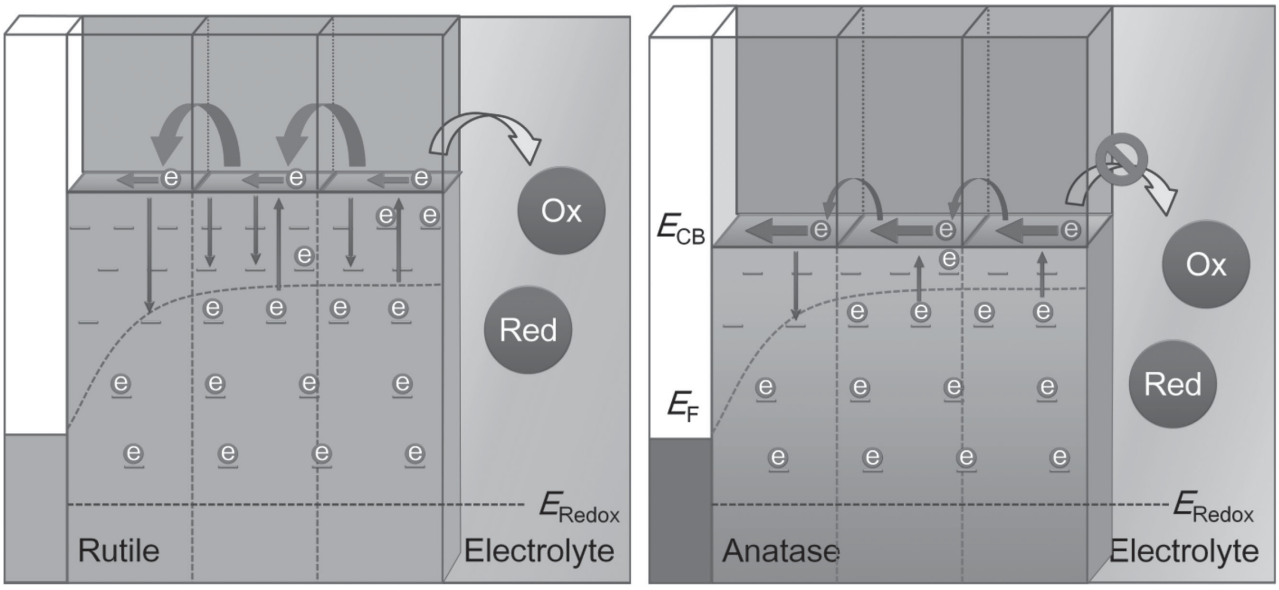

Figure 4. Schematic illustration of the features of electronic processes occurring in rutile (left) and anatase (right) TiO_2-based photoelectrochemical cells. As illustrated in the schemes, the trap-free diffusion of electrons in the conduction band consists of two parts, i.e., the internal electron movement and intergrain charge transfer, which are connected in series. Although the internal electron movement in anatase TiO_2 is faster than that in rutile polymorph, the intergrain charge transfer is not as efficient as that in rutile TiO_2. As a result, the D_0 values for these two electrodes are very similar (Figure 2). Despite a similar D_0 value, the higher density of trap sites in the band gap of the rutile electrode increases the probability of trapping/detrapping events during the charge transport, resulting in lowering of charge diffusion coefficient (Figure S8, Supporting Information). Moreover, the higher density of trap states in the rutile electrode will aggravate the interfacial charge recombination (Figure S9, Supporting Information). The straight arrows represent the internal electron movement inside the building blocks, while the curved arrows show the intergrain charge transfer during the charge transport procedures.

interior (internal electron movement) of the building blocks and the grain boundaries (intergrain charge transfer), it can be modeled as being connected in series and the trap-free diffusion coefficient in nanostructured electrodes (or the mobility) can be expressed as

$$\frac{1}{D_0} = \frac{1}{D_{0,\mathrm{in}}} + \frac{1}{D_{0,\mathrm{ex}}} \tag{3a}$$

where $D_{0,\mathrm{in}}$ and $D_{0,\mathrm{ex}}$ are trap-free diffusion coefficients of charges in the interior of the semiconductor and across grain boundaries, respectively. Therefore, the mobility of charges (μ) in each element can be described as

$$\frac{1}{\mu} = \frac{1}{\mu_{\mathrm{in}}} + \frac{1}{\mu_{\mathrm{ex}}} \tag{3b}$$

where μ_{in} and μ_{ex} describe the charge mobility in the interior of the semiconductor and across grain boundaries, respectively. In our system, a similar D_0 value for the two electrodes (anatase and rutile TiO_2; Figure 2) can be interpreted as the following: although the electron mobility in the interior of rutile crystal is smaller than that in the anatase counterpart ($D_{0,\mathrm{in,rutile}} < D_{0,\mathrm{in,anatase}}$), the more efficient intergrain charge transfer ($D_{0,\mathrm{ex,rutile}} > D_{0,\mathrm{ex,anatase}}$) can compensate for the shortage of intrinsic internal charge movement and bring the total charge mobility in the rutile electrode up to a similar value as the anatase electrode. To further verify our assumption, we investigated the effect of intergrain necking conditions on the transport of charges in TiO_2 electrodes. In order to obtain the insightful information on the impact of necking condition (related to $D_{0,\mathrm{ex}}$) while keeping the internal charge movement ($D_{0,\mathrm{in}}$) unchanged, we managed to change the features of necking area and coordination number by changing the porosity of the TiO_2 electrodes. By plotting the trap-free diffusion parameters over the porosity (**Figure 5**a), it can be seen that the influence of porosity on D_0 is much more significant for the anatase electrode. The sensitive variation of D_0 over the porosity suggests that in anatase electrode, the intergrain charge transfer plays a more predominant role on charge transport than the rutile counterpart. Associated with the fact of faster internal electron movement in the anatase TiO_2[22] and a similar value of D_0 for the anatase and rutile TiO_2 electrodes (Figure 2), it is expected that the intergrain charge transfer will be more efficient in the rutile electrode.

2.3.2. Improvement of Charge Mobility by Composition

Since the shape and size for both of the rutile and anatase TiO_2 nanostructures are similar, and the technique parameters (e.g., solid concentration of TiO_2 in the paste, ramping temperature, heating duration at the desired temperature, and cooling) used for the fabrication of porous electrodes are the same, it is expected that the architectural features of resultant films would be identical. Our anticipation was further verified by the nitrogen adsorption–desorption and dye desorption measurements, which showed that the semiconductor electrodes made of these two polymorphs of TiO_2 nanostructures have similar pore distributions and surface area for dye loading (Figure S7,

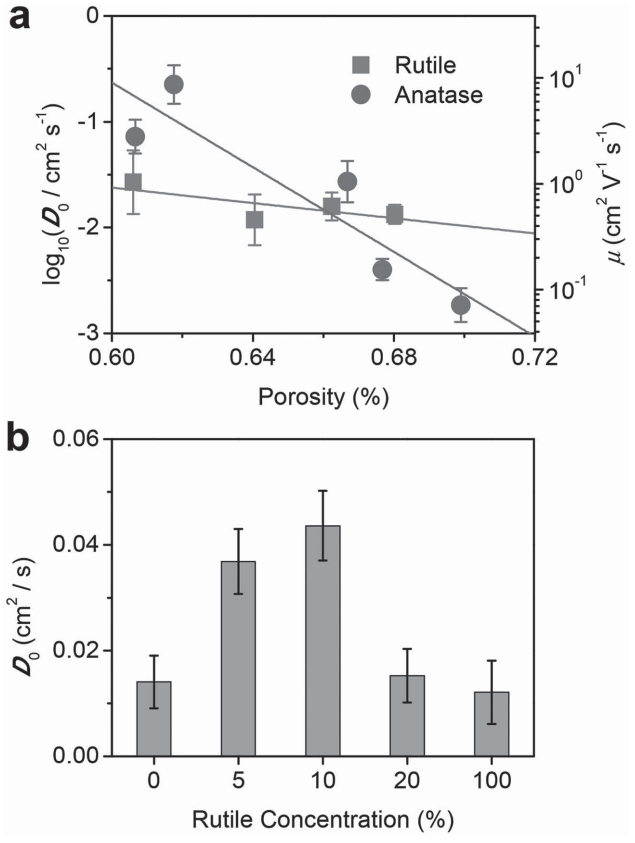

Figure 5. Porosity- and intergradient-dependent trap-free diffusion coefficient of electrons in the porous semiconductor electrodes. a) Trap-free diffusion coefficient of electrons in rutile and anatase TiO_2-based electrodes with various porosities. b) Trap-free diffusion coefficient of electrons in TiO_2 electrodes composed of mixed phases of rutile and anatase.

Supporting Information). Similar trap-free diffusion coefficient and mobility of charges (Figure 2) in the electrodes made of rutile and anatase TiO_2 are most likely resulted from the more efficient intergrain charge transfer between building blocks in the rutile electrodes. By introducing rutile TiO_2 into anatase nanostructured electrodes, the better intergrain connectivity can help to improve the charge transfer between the building blocks made of these two polymorphs. Therefore, the anatase building blocks in the mesoporous electrodes can be bridged by the rutile nanostructures. This conclusion is further verified by the fact that the mobility of electrons is improved in the electrodes made of mixed phases of rutile and anatase (Figure 5b). Although the position of conduction band edge of rutile TiO_2 is slightly higher than that of anatase TiO_2, which makes the electrons in the phase-mixed electrodes consume additional energy to overcome the barriers during the charge transport, the benefit resulted from the promotion of intergrain connectivity in phase-mixed electrodes is obviously greater than those unfavorable energy dissipations.

The higher value of trap-free diffusion coefficient is beneficial for the charge transport when the concentration of charges in the semiconductor electrodes is high. However, the situation is not always delightful.[8d] According to the MT model, lowering the concentration of photoinduced charge carriers rapidly decreases the charge diffusion coefficient. For a semiconductor electrode with higher density of trap states in the band gap, it requires much more free electrons to keep a desired charge diffusion coefficient. As a result, a semiconductor electrode with high charge mobility still exhibits the relatively low charge diffusion coefficient if the concentration of charge carriers in it is not high enough.[8d,8f] In our system, when the concentration of photoinduced charge carriers is high, the improved intergrain connectivity benefited from the introduction of the rutile building blocks can facilitate the transport of charges in the electrode made of phase-mixed TiO_2 (90% anatase and 10% rutile) (Figure S12, Supporting Information). However, the charge diffusion rate decreases rapidly as the illumination intensity goes down. The charge diffusion coefficient of the phase-mixed TiO_2 electrode becomes even smaller than that of pure anatase electrode at low concentration of photogenerated charge carriers (Figure S12, Supporting Information). Since the photogenerated electrons have to pass the rutile building blocks in the phase-mixed electrodes before they reach the conducting substrate, the higher density of trap states in rutile building blocks will increase the probability of trapping/detrapping events, resulting undesirably in decrease of charge diffusion coefficient. This will also decrease the charge collection efficiency and thus the performances of the photovoltaic devices made of these electrodes (Figure S13, Supporting Information).

2.3.3. Bridging and Fencing Electron Highways by Surface Rutilization

In order to alleviate the trapping/detrapping events while fully exerting the benefit of improved intergrain connectivity, it is desired to reduce the travel distance of electrons in the rutile building blocks. To achieve this goal, formation of thin rutile layers between the adjacent anatase building blocks should be beneficial. Toward this end, we developed a facile surface rutilization method to in situ form a homogeneous thin rutile layer on anatase nanostructures to minimize the internal energy dissipation. Surface rutilization of anatase TiO_2 was realized by hydrothermal treatment of anatase nanostructures in HCl solution (**Figure 6**a,b and Figure S14, Supporting Information). Features, including crystallinity and thickness of rutilized thin layer could be adjusted by changing the reaction time and temperature (Figure S14, Supporting Information).

With the rutilized surface, the intergrain charge transfer between adjacent anatase building blocks can be bridged in the nanostructured TiO_2 electrodes. As determined by impedance spectroscopy, the trap-free diffusion coefficient of electrons in this kind of electrodes reaches as high as 0.148 cm^2 s^{-1} (Figure 6c), which is about ten time higher than that obtained in the pure anatase TiO_2 electrode (0.0147 cm^2 s^{-1}; Figure 2). Besides, because of the promising band alignment, the isolation of exposed anatase phase to the electrolyte by the formed rutilized thin layers can effectively retard the electrons in the nanostructured electrodes from recombination with oxidized species on the SEI (Figure S15, Supporting Information), which can further improve the charge collection efficiency (Figure S16, Supporting Information). Since the rutile layer is ultrathin (≈1–4 nm; Figure 6 and Figures S12 and S17,

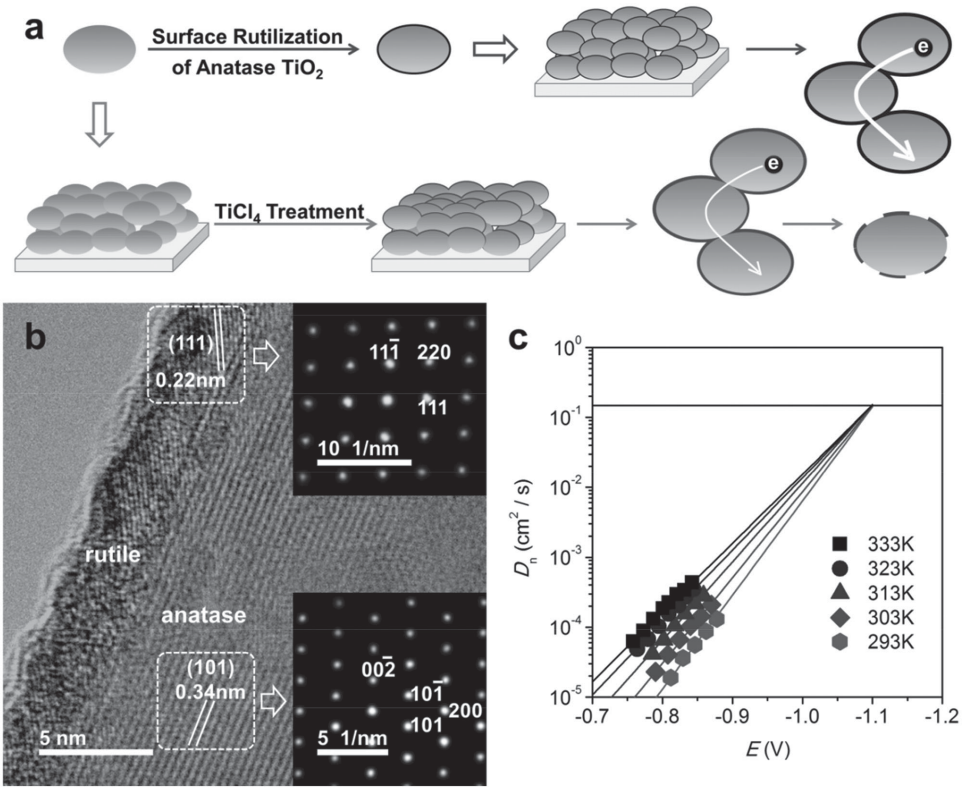

Figure 6. Features of semiconductor electrodes based on surface rutilized anatase nanostructures. a) Schematic illustration of the fabrication of TiO_2 electrodes using surface rutilized anatase nanostructures (top). For comparison, the common technique used for $TiCl_4$ treatment of TiO_2 electrode is also presented (bottom). It can be seen that the intergrain connectivity between adjacent building blocks is rather different for electrodes fabricated by these two routes. For the electrodes using surface rutilized TiO_2 (top), the adjacent anatase building blocks are intermediated by the thin rutilized layer. For the $TiCl_4$ treated electrodes (bottom), the treatment just modifies the exposed surface; while the intergrain connectivity remains unchanged. By extracting the individual building block from the $TiCl_4$ treated electrode, it can be seen that the particles are only partially and loosely coated by the formed TiO_2 layers (bottom), which is quite different from the situation of fully coated rutilized layers in our system (top). b) HRTEM image showing the formation of a rutilized thin layer on the surface of anatase TiO_2 nanorods. Insets show the SAED patterns taken on the surface (top) and bulk (bottom) of the TiO_2 nanostructures. The surface coating layer looks different from the bulk crystal, suggesting the phase transformation occurring on the surface of the TiO_2 nanostructures (the change and transformation of the surface features are specifically shown in Figure S14, Supporting Information). The SAED pattern (upper, inset) obtained on the surface of the nanostructures matches well with the reciprocal lattice of rutile along the [1–10] zone axis. The lattice fringes on the surface of the nanostructures are also very close to the (111) interplanar spacing of rutile TiO_2. Besides, XRD patterns (Figure S14, Supporting Information) further confirm that the newly formed phase is of rutile TiO_2. c) Temperature-dependent diffusion coefficients of electrons in the electrodes composed of surface rutilized anatase TiO_2 nanostructures. The trap-free diffusion coefficient of electrons in this type of electrodes reaches as high as 0.148 $cm^2\ s^{-1}$, which is most likely resulted from the excellent electronic connectivity between adjacent building blocks, and provides the efficient intergrain charge transfer for transport of charges in the porous electrodes.

Supporting Information), the significant reduction of electron travel distance in the interior of rutile TiO_2 can accelerate the total charge diffusion. Besides, the relatively lower probability of trapping/detrapping events in the electrodes based on surface rutilized anatase TiO_2 nanostructures can further improve the charge transport even at low density of photogenerated electrons (Figure S12, Supporting Information).

Our strategy is rather different from the case of commonly adopted $TiCl_4$ post-treated TiO_2 electrodes in DSSCs. The main purpose for heterogeneous $TiCl_4$ post-treatment is to form TiO_2 coatings on the electrode surface, which would be beneficial to the charge collection by blocking the interfacial charge transfer.[23] From the viewpoint of electrode configuration, the $TiCl_4$ post-treatment only forms thin TiO_2 coatings on the "exposed" surface of the porous electrodes (Figure 6a), rather than fully coating the surface of the building blocks. Therefore, the improvement in the intergrain charge transfer would be tiny, due to the absence of the bridging rutilized thin layer between adjacent anatase building blocks. As estimated from the temperature-dependent D_n, the trap-free diffusion coefficient of electrons in the $TiCl_4$ post-treated TiO_2 electrode is 0.0175 $cm^2\ s^{-1}$ (Figure S18, Supporting Information), which is quite similar to that of the untreated electrode (0.0147 $cm^2\ s^{-1}$; Figure 2). In our case, the anatase nanostructures were completely coated by the rutilized surface thin layers prior to fabricate the electrodes, which are quite similar to the anatase@rutile core–shell structures. Therefore, in the formed electrodes, the connectivity between adjacent anatase building blocks can be significantly improved by the bridging rutilized thin layer, which can facilitate the intergrain charge transfer (Figure 6).

By virtue of these merits, the PEC devices fabricated by this kind of TiO_2 electrodes exhibit better performance. Our

hypothesis was well supported by the photovoltaic characteristics of the DSSCs assembled from these TiO_2 materials (Figure S19, Supporting Information). The photocurrent–voltage characteristics show that J_{SC} and the energy conversion efficiency for the cell made of surface rutilized anatase TiO_2 electrode are 16.65 mA cm^{-2} and 9.62%, respectively, which are much higher than those for the cell with plain anatase nanostructures (Figure S11, Supporting Information).

3. Conclusion

We have demonstrated that in nanostructured TiO_2 electrodes, the internal movement of electrons is faster inside anatase building blocks, while the rutile counterparts exhibit more efficient intergrain charge transfer. As a result, introduction of rutile into the TiO_2 electrodes can improve the charge mobility by facilitating the intergrain charge transfer between the adjacent building blocks, although the conduction band edge of rutile TiO_2 as we observed is slightly higher than that of anatase polymorph. To reduce the energy dissipation by the trapping/detrapping events in rutile TiO_2 and improve the charge collection by retarding the interfacial charge recombination, simultaneously bridging the intergrain charge transfer and fencing electron highways in nanostructured anatase TiO_2 electrodes are realized by using the surface rutilized anatase nanostructures as the building blocks. The significance of this work lies in the successful demonstration of redox couple based PEC cells. Furthermore, we believe that our work can also prompt the sequential development of solar water splitting cells, perovskite solar cells, energy storage devices, and other relevant applications.

4. Experimental Section

Preparation of TiO_2 Materials: Anatase TiO_2 nanorods were synthesized based on our previously reported method with slight modification.[10b] Briefly, 3.2 g of NH_4Cl (Merck) was firstly dissolved in 32 mL of isopropanol (Pr^iOH, Fisher Scientific, assay: >99.5%, water: <0.2%) in a Teflon-lined stainless-steel autoclave (100 mL). The mixture was stirred at ambient condition for 5 min before addition of 2 mL of titanium (IV) tetraisopropoxide (Sigma-Aldrich, 97%). After stirring for 30 min, 40 mL of (diluted) ammonia water was added. To tune the aspect ratios of the anatase nanorods, the (diluted) ammonia water with various concentrations was used. The volume ratios of commercially available ammonia water (28%–30%) to the diluting water were 0:1, 1:4, 2:3, and 1:0. After stirring for another 5 min, the autoclave was sealed and kept at 170 °C for 72 h, and the resulting precipitates were collected and washed with deionized water for three times and then ethanol for three times. The rutile TiO_2 nanorods were synthesized by one-step hydrothermal treatment of $TiCl_4$ solution. Briefly, 15 mL of $TiCl_4$ solution (2.5 M; Merck) was added into 60 mL of water in a 200 mL flask under stirring. The obtained clear solution was then heated to 90 °C and kept for 2 h. After that, the slurry was transferred into a sealed Teflon-lined autoclave which was heated at 160 °C for 12 h to grow rutile TiO_2 nanorods. Surface rutilization of anatase TiO_2 nanorods was realized by hydrothermal treatment of the anatase TiO_2 nanorods in HCl solution (6 M) at 180–200 °C for 24–72 h.

Fabrication of Sandwich-Type Cells: The TiO_2 paste with rutile or anatase nanorods was prepared by ultrasonically dispersing the TiO_2 nanostructures in the mixture of water and ethanol (v:v = 1:1). After sonication, the solid was collected by centrifugation and dried overnight under vacuum at 90 °C. The TiO_2 paste was prepared by dispersing the dried nanostructures (450 mg) into 2.5 mL of terpineol (Sigma-Aldrich) under stirring. Prior to addition of the dried TiO_2 powders, certain amount (typically 225 mg) of ethyl cellulose (Sigma-Aldrich) was dissolved into the terpineol to tune the viscosity of the paste and the porosity of the final sintered TiO_2 films. The TiO_2 paste was then deposited on fluorine-doped tin oxide conducting glass substrate (FTO; 14 Ω $square^{-1}$, Nippon Sheet Glass) by screen printing (Safer, Polyester, 250 meshes). Then the film was heated to 500 °C at a rate of 15 °C min^{-1} and kept for 30 min. After cooling down to 80 °C, the TiO_2 electrode was immersed overnight in an N719 dye (Dyesol) solution (0.5×10^{-3} M). The electrode was then rinsed with acetonitrile and dried. Subsequently, the sensitized TiO_2 film was assembled with a platinized FTO glass into sealed sandwich-type cell by heating with a Surlyn film (60 μm in thickness). After that, one drop of electrolyte was filled into the interelectrode space by vacuum injection. The electrolyte was composed of 0.1 M of lithium iodide (Sigma-Aldrich), 0.6 M of tetrabutylammonium iodide (Sigma-Aldrich), 0.05 M of iodine (I_2; Sigma-Aldrich), and 0.5 M of 4-*tert*-butylpyridine (Sigma-Aldrich) in acetonitrile.

Electrochemistry and Photoelectrochemistry: The electronic processes occurring in the semiconductor electrodes were mainly characterized by impedance spectroscopy, which was performed with a computer controlled Solartron potentiostat with a frequency range of 500 k–0.05 Hz. The amplitude of the AC signal was 10 mV. The obtained spectra were fitted with Z-view software. Electron transport resistance (R_t), interfacial charge recombination resistance (R_{ct}), and chemical capacitance (C_μ) can be obtained from the fitting results. The electronic conductivity (σ) of TiO_2 network can be calculated from R_t by using the geometrical parameters. And the electronic process features, such as lifetime (τ_n), diffusion coefficient (D_n), and diffusion length (L_n) of electrons in the semiconductor electrode, can be calculated by the following equations

$$\tau_n = R_{ct} C_\mu \tag{4}$$

$$D_n = \frac{1}{R_t C_\mu} = \frac{\sigma}{C_\mu} \tag{5}$$

$$L_n = \sqrt{\sigma R_{ct}} = \sqrt{D_n \tau_n} \tag{6}$$

Determination of electron diffusion coefficient at various illumination intensities was carried out by stepped light-induced transient measurement of photocurrents.[24] The time constant was obtained by fitting the decay of the photocurrent transient to the function of $\exp(-t/\tau_c)$, where t is time and τ_c is the time constant for electron collection. The values of D_n can be obtained using the following equation

$$D_n = d^2/(2.35 * \tau_c) \tag{7}$$

where d is the thickness of the semiconductor film. The retarding of interfacial charge recombination by the rutilized surface was also determined by open-circuit voltage decay spectroscopy, which monitored the variation of electrode potentials over the time. The time constant (τ_n) for charge recombination can be obtained from the following equation[25]

$$\tau_n = -\frac{k_B T}{q}\left(\frac{dV_{OC}}{dt}\right)^{-1} \tag{8}$$

where k_B is the Boltzmann constant, T is the temperature, and q is the elementary charge. The photovoltaic behaviors of the sandwich-type cells were characterized by recording the photocurrent–voltage (J–V) curves under A.M. 1.5 G illumination (100 mW cm^{-2}). The illumination was provided from an ABET solar simulator.

Materials Characterization: The TiO_2 nanostructures were characterized by XRD using a Bruker D8 X-ray powder diffractometer. TEM and high-resolution TEM (HRTEM) investigations were taken with a JEOL JEM-2010 field emission electron microscope operated at 200 kV. The SAED patterns of samples were obtained by the fast Fourier transform of the HRTEM image using DigitalMicrograph software (Gatan). Morphology of the samples was characterized by FESEM on a JEOL JSM-6701F

electron microscope. Porosity of the TiO_2 was measured using a nitrogen adsorption/desorption method on Quantachrome Autosorb-6 (AS6). The amount of dye uptake on the semiconductor electrodes was measured by dye desorption in ethanolic solution containing 0.1 M NaOH. The absorbance of the resulting solution was measured by UV–visible spectrophotometry (Varian Cary 4000).

Supporting Information

Supporting Information is available from the Wiley Online Library or from the author.

Acknowledgements

This work was supported by Nanyang Technological University (M4080977.120.50000), Ministry of Education of Singapore (M4011021.120) under Academic Research Fund (AcRF) Tier 2 (ARC 26/13, No. MOE2013-T2-1-034; ARC 19/15, No. MOE2014-T2-2-093), AcRF Tier 1 (RG 9/12, RG 61/12, RGT18/13, and RG5/13), and Start-Up grant (M4081296.070.500000), A*Star (M4070178.120), and the Singapore-Berkeley Research Initiative for Sustainable Energy (SinBeRISE). This research was also conducted at Nanyang Technological University–Hebrew University of Jerusalem–Ben-Gurion University Nanomaterials for Energy and Water Management Programme under the Campus for Research Excellence and Technological Enterprise, which was supported by the National Research Foundation, Prime Minister's Office, Singapore. One of the authors, J.C., thanks Dr. Yinghua Xu (Zhejiang University of Technology) and Dr. Tiancheng Xu (HzCell Electrochem. Corp.) for the help with discussion of impedance results.

Received: September 26, 2015
Revised: October 13, 2015
Published online: December 9, 2015

[1] a) M. Gratzel, *Nature* **2001**, *414*, 338; b) X. Chen, S. S. Mao, *Chem. Rev.* **2007**, *107*, 2891; c) A. Fujishima, K. Honda, *Nature* **1972**, *238*, 37.
[2] a) R. I. Bickley, T. Gonzalez-Carreno, J. S. Lees, L. Palmisano, R. J. D. Tilley, *J. Solid State Chem.* **1991**, *92*, 178; b) Y. K. Kho, A. Iwase, W. Y. Teoh, L. Mädler, A. Kudo, R. Amal, *J. Phys. Chem. C* **2010**, *114*, 2821; c) T. Ohno, K. Tokieda, S. Higashida, M. Matsumura, *Appl. Catal. A* **2003**, *244*, 383.
[3] G. Li, K. A. Gray, *Chem. Phys.* **2007**, *339*, 173.
[4] T. Luttrell, S. Halpegamage, J. G. Tao, A. Kramer, E. Sutter, M. Batzill, *Sci. Rep.* **2014**, *4*, 4043.
[5] a) D. C. Hurum, A. G. Agrios, K. A. Gray, T. Rajh, M. C. Thurnauer, *J. Phys. Chem. B* **2003**, *107*, 4545; b) D. O. Scanlon, C. W. Dunnill, J. Buckeridge, S. A. Shevlin, A. J. Logsdail, S. M. Woodley, C. R. A. Catlow, M. J. Powell, R. G. Palgrave, I. P. Parkin, G. W. Watson, T. W. Keal, P. Sherwood, A. Walsh, A. A. Sokol, *Nat. Mater.* **2013**, *12*, 798; c) L. Kavan, M. Gratzel, S. E. Gilbert, C. Klemenz, H. J. Scheel, *J. Am. Chem. Soc.* **1996**, *118*, 6716.
[6] A. Hagfeldt, G. Boschloo, L. C. Sun, L. Kloo, H. Pettersson, *Chem. Rev.* **2010**, *110*, 6595.
[7] A. J. Frank, N. Kopidakis, J. van de Lagemaat, *Coord. Chem. Rev.* **2004**, *248*, 1165.
[8] a) N. Kopidakis, E. A. Schiff, N. G. Park, J. van de Lagemaat, A. J. Frank, *J. Phys. Chem. B* **2000**, *104*, 3930; b) L. Dloczik, O. Ileperuma, I. Lauermann, L. M. Peter, E. A. Ponomarev, G. Redmond, N. J. Shaw, I. Uhlendorf, *J. Phys. Chem. B* **1997**, *101*, 10281; c) E. Hendry, M. Koeberg, B. O'Regan, M. Bonn, *Nano Lett.* **2006**, *6*, 755; d) J. Villanueva-Cab, S.-R. Jang, A. F. Halverson, K. Zhu, A. J. Frank, *Nano Lett.* **2014**, *14*, 2305; e) J. E. Kroeze, T. J. Savenije, J. M. Warman, *J. Am. Chem. Soc.* **2004**, *126*, 7608; f) K. Zhu, N. R. Neale, A. Miedaner, A. J. Frank, *Nano Lett.* **2007**, *7*, 69.
[9] a) E. Palomares, J. N. Clifford, S. A. Haque, T. Lutz, J. R. Durrant, *J. Am. Chem. Soc.* **2003**, *125*, 475; b) J. R. Durrant, S. A. Haque, E. Palomares, *Coord. Chem. Rev.* **2004**, *248*, 1247.
[10] a) J. van de Lagemaat, K. D. Benkstein, A. J. Frank, *J. Phys. Chem. B* **2001**, *105*, 12433; b) J. Chen, H. B. Yang, J. Miao, H.-Y. Wang, B. Liu, *J. Am. Chem. Soc.* **2014**, *136*, 15310.
[11] a) J. Livage, M. Henry, C. Sanchez, *Prog. Solid State Chem.* **1988**, *18*, 259; b) M. Henry, J. Jolivet, J. Livage, in *Chemistry, Spectroscopy and Applications of Sol-Gel Glasses*, Vol. *77* (Eds: R. Reisfeld, C. K. Jjørgensen), Springer, Berlin Heidelberg, Germany **1992**, p. 153.
[12] F. Fabregat-Santiago, J. Bisquert, G. Garcia-Belmonte, G. Boschloo, A. Hagfeldt, *Sol. Energy Mater. Sol. Cells* **2005**, *87*, 117.
[13] a) J. Bisquert, *J. Phys. Chem. B* **2001**, *106*, 325; b) F. Fabregat-Santiago, G. Garcia-Belmonte, J. Bisquert, A. Zaban, P. Salvador, *J. Phys. Chem. B* **2002**, *106*, 334; c) F. Fabregat-Santiago, J. Bisquert, E. Palomares, L. Otero, D. B. Kuang, S. M. Zakeeruddin, M. Grätzel, *J. Phys. Chem. C* **2007**, *111*, 6550.
[14] J. Bisquert, *Phys. Chem. Chem. Phys.* **2008**, *10*, 49.
[15] I. Abayev, A. Zaban, F. Fabregat-Santiago, J. Bisquert, **2003**, *196*, R4.
[16] F. Fabregat-Santiago, J. Bisquert, L. Cevey, P. Chen, M. K. Wang, S. M. Zakeeruddin, M. Grätzel, *J. Am. Chem. Soc.* **2009**, *131*, 558.
[17] J. Bisquert, V. S. Vikhrenko, *J. Phys. Chem. B* **2004**, *108*, 2313.
[18] V. Pfeifer, P. Erhart, S. Li, K. Rachut, J. Morasch, J. Brötz, P. Reckers, T. Mayer, S. Rühle, A. Zaban, I. Mora Seró, J. Bisquert, W. Jaegermann, A. Klein, *J. Phys. Chem. Lett.* **2013**, *4*, 4182.
[19] a) T. Tiedje, J. M. Cebulka, D. L. Morel, B. Abeles, *Phys. Rev. Lett.* **1981**, *46*, 1425; b) J. Orenstein, M. Kastner, *Phys. Rev. Lett.* **1981**, *46*, 1421.
[20] a) A. Hagfeldt, M. Graetzel, *Chem. Rev.* **1995**, *95*, 49; b) J. van de Lagemaat, A. J. Frank, *J. Phys. Chem. B* **2000**, *104*, 4292; c) D. Cahen, G. Hodes, M. Grätzel, J. F. Guillemoles, I. Riess, *J. Phys. Chem. B* **2000**, *104*, 2053.
[21] N. Kopidakis, N. R. Neale, A. J. Frank, *J. Phys. Chem. B* **2006**, *110*, 12485.
[22] a) H. Tang, K. Prasad, R. Sanjinès, P. E. Schmid, F. Lévy, *J. Appl. Phys.* **1994**, *75*, 2042; b) L. Forro, O. Chauvet, D. Emin, L. Zuppiroli, H. Berger, F. Lévy, *J. Appl. Phys.* **1994**, *75*, 633.
[23] S. Ito, P. Liska, P. Comte, R. Charvet, P. Pechy, U. Bach, L. Schmidt-Mende, S. M. Zakeeruddin, A. Kay, M. K. Nazeeruddin, M. Grätzel, *Chem. Commun.* **2005**, 4351.
[24] S. Nakade, T. Kanzaki, Y. Wada, S. Yanagida, *Langmuir* **2005**, *21*, 10803.
[25] A. Zaban, M. Greenshtein, J. Bisquert, *ChemPhysChem* **2003**, *4*, 859.